JOURNAL OF THERMOPHYSICS AND HEAT TRANSFER
Vol. 13, No. 3, July–September 1999

Mixed Convective Boiling Heat Transfer in a Vertical Capillary Structure Heated Asymmetrically

T. S. Zhao* and Q. Liao†
Hong Kong University of Science and Technology, Clear Water Bay, Kowloon, Hong Kong, People's Republic of China

Mixed convective boiling heat transfer in a vertically oriented capillary porous structure with asymmetric heating of opposing walls is numerically investigated using a multiphase mixture model. Liquid-saturation distributions, isotherms, as well as liquid and vapor velocity fields subjected to both superimposed aiding and opposing flows, are analyzed and presented. The liquid velocity distributions for both aiding and opposing flows indicate the existence of a secondary convective cell adjacent to the cold wall when the strength of the imposed flow is small. It is found that for the case of an aiding flow, the minimum liquid saturation always occurs at the exit of the packed channel. For the case of an opposing flow, however, the minimum liquid saturation usually locates in the middle part of the heated surface and the area of the minimum liquid saturation expands upward as the strength of the imposed opposing flow is weakened. The effect of particle diameters on the minimum liquid saturation along the heated wall is also examined.

Nomenclature

c = specific heat, J/(kg K)
$D(s)$ = capillary diffusion coefficient, m^2/s
$f(s)$ = hindrance function
g = gravitational acceleration, m/s^2
H = pseudomixture enthalpy, J/m^3
h = enthalpy, J/kg
h_{fg} = latent heat of liquid/vapor phase change, J/kg
$J(s)$ = capillary pressure function
j = diffusive mass flux, $kg/(m^2\ s)$
K = absolute permeability, m^2
k_{eff} = effective thermal conductivity, W/(m K)
k_r = relative permeability
L = height of the capillary structure, mm
p = pressure, N/m^2
q_w = imposed heat flux, W/m^2
s = liquid saturation
T = temperature, K
$\boldsymbol{u}$ = superficial or Darcian velocity vector, m/s
W = width of the capillary structure, mm
x = coordinate in vertical direction
y = coordinate in horizontal direction
β = thermal expansion coefficient, 1/K
Γ_h = effective diffusion coefficient, m^2/s
γ_h = two-phase advection correction coefficient
$\Delta\rho$ = density difference, $\rho_l - \rho_v$, kg/m^3
ε = porosity
λ = relative mobility
μ = viscosity, N s/m^2
ν = kinetic viscosity, m^2/s
ρ = density, kg/m^3
σ = surface tension, N/m
Ω = effective heat capacitance ratio

Subscripts

c = capillary or cold wall
h = heating
in = inlet
ir = irreducible
k = kinetic property
l = liquid phase
s = solid phase
sat = saturated state
v = vapor phase

Received 6 August 1998; revision received 3 February 1999; accepted for publication 4 February 1999.

*Assistant Professor, Department of Mechanical Engineering.
†Research Associate, Department of Mechanical Engineering.

Introduction

MIXED convective heat transfer in a liquid-saturated porous media-packed channel has been a subject of intensive study during the last two decades. For example, Wooding[1] and Sutton[2] conducted theoretical studies on the onset of free convection in porous channels. Lai et al.[3] numerically investigated the aiding and opposing mixed convective flows in a vertical porous layer for the case when a finite isothermal heat source is located on a vertical wall while the other wall is isothermally cooled. They found that a circulatory secondary flow exists. For an aiding flow the heat transfer rate increases monotonically with the aiding velocity. For the opposing flow with increasing Peclet numbers the heat transfer rate first decreases and reaches a minimum before starting to increase again. Choi et al.[4] presented their numerical and experimental results on mixed convection through vertical porous annuli that are heated from the inner cylinder with a constant heat flux. They found that the heat transfer is enhanced as the strength of either imposed flow or buoyancy-induced flow increases for the aiding flow; whereas for the opposing flow, heat transfer coefficient decreases with the increase of the imposed flow strength. Pu et al.[5] reported their experimental results of mixed convection heat transfer in a vertical packed channel with asymmetric heating of opposing walls. Their measurements of the temperature distribution indicates the existence of a secondary convective cell inside the vertical packed channel in the mixed convection regime. The previously mentioned review of literature reveals that most of the studies on mixed convection in porous media are confined to liquid saturate or single-phase flows.

In this work, mixed convective boiling heat transfer in a vertically oriented capillary porous structure with asymmetric heating of opposing walls was numerically investigated using the multiphase mixture model.[6–10] The objective is to study the influence of both aiding and opposing flows on the flowfield and the associated heat transfer characteristics in such a system. Of special interest are the cases where the strengths of the buoyancy-induced upflow and the superimposed downflow are approximately the same, such that a convective secondary cell forms adjacent to the cold wall. It is shown that for the case of aiding flows, the minimum liquid saturation always occurs at the exit of the packed channel. However, for the case

of opposing flows, the minimum liquid saturation usually locates in the middle part of the heated wall and it moves upward along the wall as the strength of the imposed opposing flow is reduced. The effect of particle diameters on the minimum liquid saturation along the heated wall is also examined.

Formulation

Consider a two-dimensional vertical capillary porous medium structure ($W \times L$), as depicted in Fig. 1, whose right sidewall is heated at a constant heat flux q_w, whereas the opposing wall (the left side) is cooled at a constant temperature T_c. The porous medium is assumed to be homogeneous, isotropic, and fully saturated with fluid. Either an aiding (Fig. 1a) or an opposing (Fig. 1b) pressure-driven external flow of subcooled liquid at an inlet velocity u_{in} and a constant temperature T_c is maintained through the capillary structure. When the imposed heat flux is sufficiently high, boiling occurs on the heated surface and the thermodynamic structure of the system consists of a two-phase zone adjacent to the heated wall and a subcooled liquid zone elsewhere in the packed channel. The major assumptions and simplifications in this analysis are discussed in Ref. 6. The governing equations are given as follows:

Conservation of mixture mass:

$$\varepsilon\frac{\partial\rho}{\partial t} + \nabla\cdot(\rho\boldsymbol{u}) = 0 \tag{1}$$

Conservation of mixture momentum:

$$\boldsymbol{u} = -(K/\mu)[\nabla p - (\rho_k - \rho_o)g] \tag{2}$$

Conservation of energy:

$$\Omega\frac{\partial H}{\partial t} + \nabla\cdot(\gamma_h\boldsymbol{u}H) = \nabla\cdot(\Gamma_h\nabla H) + \nabla\cdot\left[f(s)\frac{K\Delta\rho h_{fg}}{\nu_v}g\right] \tag{3}$$

The mixture variables and properties of Eqs. (1–3) are defined as follows:

Density:

$$\rho = \rho_l s + \rho_v(1-s) \tag{4}$$

Velocity:

$$\rho\boldsymbol{u} = \rho_l\boldsymbol{u}_l + \rho_v\boldsymbol{u}_v \tag{5}$$

Pressure:

$$p = p_l + \int_0^s \lambda_v\left(\frac{\mathrm{d}p_c}{\mathrm{d}s}\right)\mathrm{d}s = p_v - \int_0^s \lambda_l\left(\frac{\mathrm{d}p_c}{\mathrm{d}s}\right)\mathrm{d}s \tag{6}$$

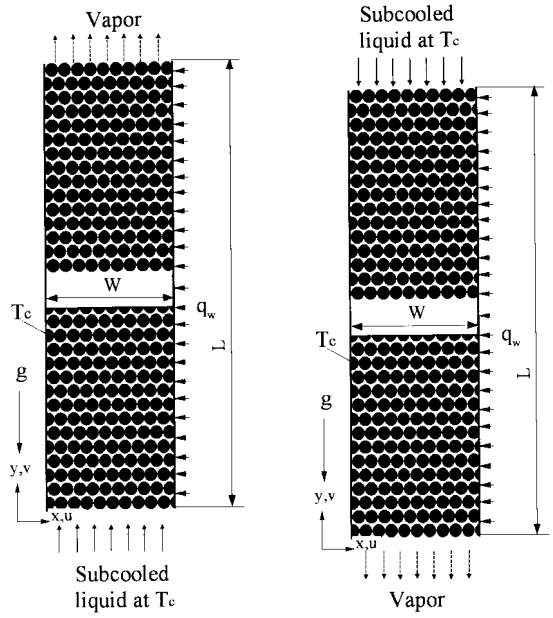

a) Aiding flows **b) Opposing flows**

Fig. 1 Schematic of the physical problem and the coordinate system.

Enthalpy:

$$H = \rho(h - 2h_{v\,\text{sat}}) \quad \text{with} \quad \rho h = \rho_l s h_l + \rho_v(1-s)h_v \tag{7}$$

Kinetic density:

$$\rho_k = \rho_l[1-\beta_l(T-T_{\text{sat}})]\lambda_l(s) + \rho_v[1-\beta_v(T-T_{\text{sat}})]\lambda_v(s) \tag{8}$$

Viscosity:

$$\mu = \frac{\rho_l s + \rho_v(1-s)}{(k_{rl}/\nu_l) + (k_{rv}/\nu_v)} \tag{9}$$

Advection correction coefficient:

$$\gamma_h = \frac{[\rho_v/\rho_l(1-s)+s][h_{v\,\text{sat}}(1+\lambda_l) - h_{l\,\text{sat}}\lambda_l]}{(2h_{v\,\text{sat}} - h_{l\,\text{sat}})s + \rho_v h_{v\,\text{sat}}(1-s)/\rho_l} \tag{10}$$

Effective heat capacitance ratio:

$$\Omega = \varepsilon + \rho_s c_s(1-\varepsilon)\frac{\mathrm{d}T}{\mathrm{d}H} \tag{11}$$

Effective diffusion coefficient:

$$\Gamma_h = \frac{1}{1+(1-\rho_v/\rho_l)h_{v\,\text{sat}}/h_{fg}}D + k_{\text{eff}}\frac{\mathrm{d}T}{\mathrm{d}H} \tag{12}$$

Capillary diffusion coefficient:

$$\mathrm{D}(s) = \frac{\sqrt{\varepsilon K}\sigma}{\mu_l}\frac{k_{rl}k_{rv}}{(\nu_v/\nu_l)k_{rl} + k_{rv}}[-J'(s)] \tag{13}$$

Relative mobility:

$$\lambda_l(s) = \frac{k_{rl}/\nu_l}{(k_{rl}/\nu_l) + (k_{rv}/\nu_v)}, \qquad \lambda_v(s) = \frac{k_{rv}/\nu_v}{(k_{rl}/\nu_l) + (k_{rv}/\nu_v)} \tag{14}$$

where the subscripts l and v denote the quantities for the liquid and vapor, respectively. The fluid temperature and liquid saturation can be recovered from the following relations:

$$T = \begin{cases} \dfrac{H + 2\rho_l h_{v\,\text{sat}}}{\rho_l c_l} & H \le -\rho_l(2h_{v\,\text{sat}} - h_{l\,\text{sat}}) \\ T_{\text{sat}} & -\rho_l(2h_{v\,\text{sat}} - h_{l\,\text{sat}}) < H \le -\rho_v h_{v\,\text{sat}} \\ T_{\text{sat}} + \dfrac{H + \rho_v h_{v\,\text{sat}}}{\rho_v c_v} & -\rho_v h_{v\,\text{sat}} < H \end{cases} \tag{15a}$$

$$s = \begin{cases} 1 & H \le -\rho_l(2h_{v\,\text{sat}} - h_{l\,\text{sat}}) \\ -\dfrac{H + \rho_v h_{v\,\text{sat}}}{\rho_l h_{fg} + (\rho_l - \rho_v)h_{v\,\text{sat}}} & -\rho_l(2h_{v\,\text{sat}} - h_{l\,\text{sat}}) < H \le -\rho_v h_{v\,\text{sat}} \\ 0 & -\rho_v h_{v\,\text{sat}} < H \end{cases} \tag{15b}$$

The liquid and vapor velocity can be calculated from the mixture velocity based on the following relations:

$$\rho_l\boldsymbol{u}_l = \lambda_l\rho\boldsymbol{u} + j, \qquad \rho_v\boldsymbol{u}_v = \lambda_v\rho\boldsymbol{u} - j \tag{16}$$

where

$$j = -\rho_l D(s)\nabla s + f(s)(K\Delta\rho/\nu_v)g \tag{17}$$

with the hindrance function $f(s)$ given by

$$f(s) = \frac{k_{rl}k_{rv}/\nu_l}{(k_{rl}/\nu_l) + (k_{rv}/\nu_v)} \tag{18}$$

In this analysis, the following constitutive relationships for the relative permeability and the capillary pressure are used[11]:

$$k_{rl}(s) = \left(\frac{s - s_{\text{ir}}}{1 - s_{\text{ir}}}\right)^3, \qquad k_{rv}(s) = \left(\frac{1-s}{1-s_{\text{ir}}}\right)^3 \tag{19}$$

$$p_c(s) = \sqrt{(\varepsilon/K)}\sigma J(s) \tag{20}$$

where

$$J(s) = 1.417(1-s) - 2.120(1-s)^2 + 1.263(1-s)^3 \tag{21}$$

The boundary conditions at $x = 0$ and W for both the aiding and the opposing flows are the same:

At $x = 0$ (left sidewall):

$$\frac{\partial p}{\partial x} = 0 \text{ (impermeable)} \tag{22}$$

$$H = \rho_l(c_l T_c - 2h_{v\,\mathrm{sat}}) \tag{23}$$

At $x = W$ (right sidewall):

$$\frac{\partial p}{\partial x} = 0 \text{ (impermeable)} \tag{24}$$

$$-\frac{\Gamma_h}{\rho}\frac{\partial H}{\partial x} = q_w \tag{25}$$

The boundary conditions at the inlet and the outlet of the packed channel are given as follows:

For the aiding flow, at $y = 0$ (inlet):

$$-\frac{\partial p}{\partial y} = \frac{\mu_l u_{\mathrm{in}}}{K} \tag{26}$$

$$H = \rho_l(c_l T_{\mathrm{in}} - 2h_{v\,\mathrm{sat}}) \tag{27}$$

At $y = L$ (outlet):

$$-\frac{\partial p}{\partial x} = 0 \text{ (fully developed flow)} \tag{28}$$

$$\frac{\partial H}{\partial y} = 0 \text{ (thermally fully developed)} \tag{29}$$

For the opposing flows, at $y = L$ (inlet):

$$-\frac{\partial p}{\partial y} = \frac{\mu_l u_{\mathrm{in}}}{K} \tag{30}$$

$$H = \rho_l(c_l T_{\mathrm{in}} - 2h_{v\,\mathrm{sat}}) \tag{31}$$

At $y = 0$ (outlet):

$$-\frac{\partial p}{\partial x} = 0 \text{ (fully developed flow)} \tag{32}$$

$$\frac{\partial H}{\partial y} = 0 \text{ (thermally fully developed)} \tag{33}$$

All of the symbols used in the governing equations and the boundary conditions are defined in the Nomenclature.

Numerical Procedure

The numerical procedure has been described in detail in Ref. 6. Using the stabilized error vector propagation method, we first solved a Possion-like equation in terms of the pressure,[6] which was obtained by substituting Eq. (2) into Eq. (1). The velocity field could be subsequently obtained from Eq. (2) after the pressure field was obtained. The energy equation was solved by a fully implicit control volume-based finite difference formulation.[12] The temperature in the single-phase region and the liquid saturation in the two-phase region could be backed out from the enthalpy field based on Eq. (15). Once a converged solution was obtained, the individual phase velocities of liquid and vapor were then determined based on Eq. (16).

The equations were solved as a simultaneous set, and convergence was achieved with the criterion that the relative errors between iterations in both the enthalpy and velocity fields be less than 10^{-5}, and that mass and energy conservation in the system was ensured to be within 0.1%. A series of test runs were performed to ensure that the numerical results were independent of the grid size. The choice of 82 × 22 uniform grid points was found to provide grid independence for the results reported in this paper.

Results and Discussion

Numerical computations were carried out for a capillary porous structure of 22 mm (W) × 120 mm (L). Glass beads of different diameters d_p, ranging from 0.5 to 1.0 mm, were chosen as the porous media, whereas water was selected as the working fluid.

The permeability was evaluated by[13]

$$K = \frac{\varepsilon^3 d_p^2}{180(1-\varepsilon)^2} \tag{34}$$

The effective thermal conductivity k_{eff} was calculated by using Zehner and Schlünder's equation[14]:

$$k_{\mathrm{eff}} = k_f\left\{1 - \sqrt{1-\varepsilon} + 2\frac{\sqrt{1-\varepsilon}}{\Lambda B}\left[\frac{(1-\Lambda)B}{(1-\Lambda B)^2}\ln\left(\frac{1}{\Lambda B}\right) - \frac{B+1}{2} - \frac{B-1}{1-\Lambda B}\right]\right\} \tag{35}$$

where $\Lambda = k_f/k_s$, with k_s and k_f being the thermal conductivity of solid and liquid phases, respectively. The shape factor B for a packed bed consisting of uniform sphere is given by

$$B = 1.25[(1-\varepsilon)/\varepsilon]^{\frac{10}{9}} \tag{36}$$

Other thermophysical properties for the water–glass bead system are listed in Table 1.

In all of the computations, the cold wall and the inlet temperatures were kept at $T_c = T_{\mathrm{in}} = 60°\mathrm{C}$.

Aiding Flow

Figures 2–4 present the distributions of the liquid saturation, the isotherms, as well as the velocities for both liquid and vapor in the capillary structure for $d_p = 0.8$ mm at $q_w = 15$ kW/m^2, as the inlet velocity of the aiding flow of a subcooled water ($s_{\mathrm{in}} = 1$) is increased from $u_{\mathrm{in}} = 0.0$ (pure natural convection) 0.08–0.3 mm/s. As shown in Figs. 2a, 3a, and 4a, at this particular value of heat flux, the two-phase zone exists in the right-upper portion of the capillary structure (represented by the variation of the gray scale from dark to light), whereas in the left-lower portion of the structure the working fluid is in the liquid phase (representing by the dark color). It is evident from Figs. 2a, 3a, and 4a that as the strength of the aiding flow becomes strong, the two-phase zone contracts while the subcooled liquid zone expands farther upstream due to the cooling effect from the incoming subcooled liquid. The isotherms shown in Figs. 2b, 3b, and 4b also indicate the existence of the two-phase zone and the subcooled liquid zone: The temperatures in the two-phase zone are at the saturated temperature (100°C), whereas the temperatures in the liquid zone are below 100°C.

The changing features of the liquid velocity fields with variations in magnitude of the imposed aiding flow are evident from Figs. 2c, 3c, and 4c. For the case of pure natural convection ($u_{\mathrm{in}} = 0.0$) the liquid adjacent to the vapor–liquid interface is heated by vapor, thus moving upward, whereas the liquid near the cold wall is cooled by the wall, thus moving downward. As a result, a closed recirculation loop (or a secondary convective cell) is formed, as shown in Fig. 2c. As the inlet liquid velocity is increased to $u_{\mathrm{in}} = 0.08$ mm/s (shown in Fig. 3c), the second convective cell still existed but became narrower and was pushed to move upward. It is interesting to note from Fig. 4c that the secondary convective cell vanishes as the inlet liquid velocity

Table 1 Thermophysical properties for the water–glass bead system

Property	Symbol	Solid	Liquid	Vapor	Unit
Density	ρ	2650	957.9	0.598	kg/m^3
Specific heat	c	1350	4.178×10^3	1.548×10^3	J/kg K
Kinetic viscosity	ν	——	4.67×10^{-7}	2.012×10^{-5}	m^2/s
Expansion coefficient	β	——	5.23×10^{-4}	2.4×10^{-3}	K^{-1}
Interfacial tension	σ	——	0.0588		N/m
Latent heat of evaporation	h_{fg}	——	2.257×10^6		J/kg

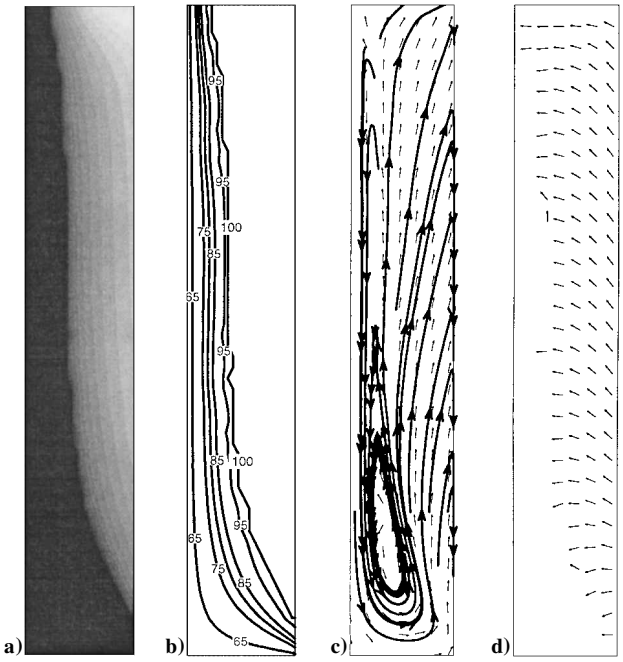

Fig. 2 Distributions of a) liquid saturation, b) isotherms (in °C), c) vapor velocity, and d) liquid velocity for the pure natural convection: $u_{in} = 0$ mm/s at $q_w = 15$ kW/m^2 and $d_p = 0.8$ mm.

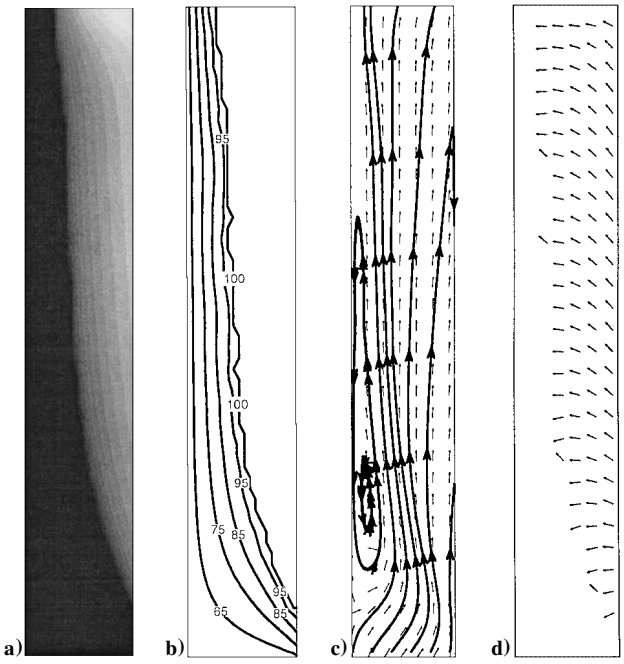

Fig. 3 Distributions of a) liquid saturation, b) isotherms (in °C), c) vapor velocity, and d) liquid velocity for the aiding flow: $u_{in} = 0.08$ mm/s at $q_w = 15$ kW/m^2 and $d_p = 0.8$ mm.

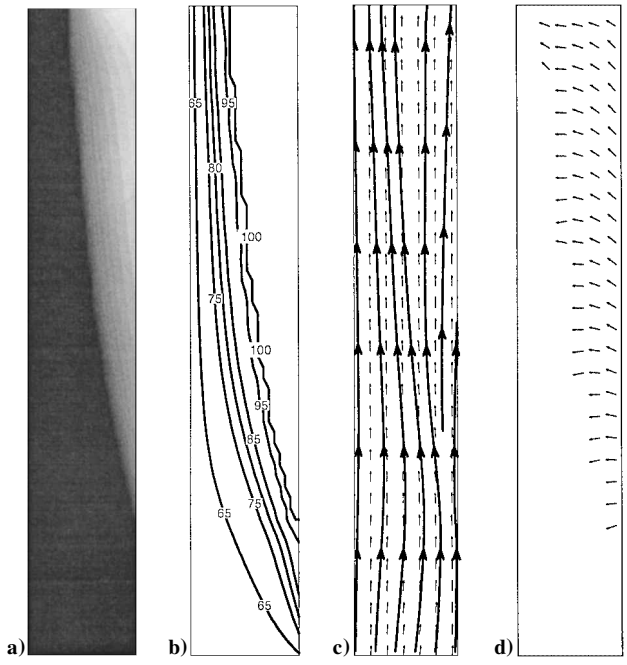

Fig. 4 Distributions of a) liquid saturation, b) isotherms (in °C), c) vapor velocity, and d) liquid velocity for the aiding flow: $u_{in} = 0.3$ mm/s at $q_w = 15$ kW/m^2 and $d_p = 0.8$ mm.

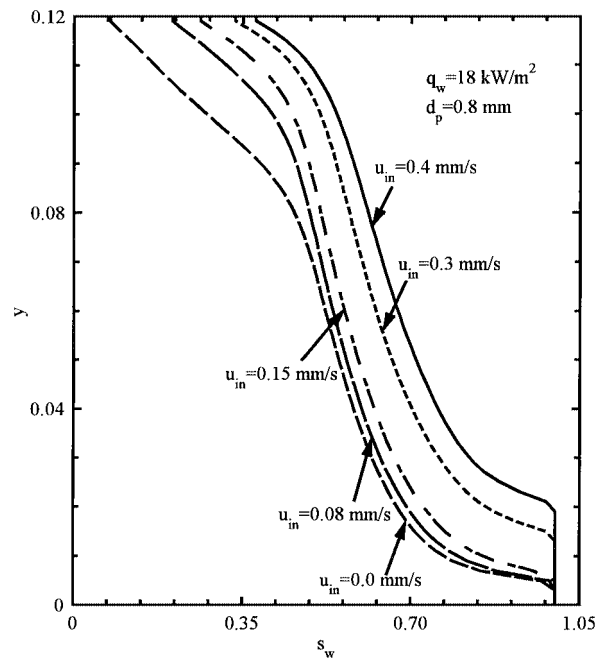

Fig. 5 Liquid saturation distribution along the heated wall for various aiding flow velocities: $u_{in} = 0.0$, 0.08, 0.15, 0.3, and 0.4 mm/s at $q_w = 18$ kW/m^2 and $d_p = 0.8$ mm.

is further increased to $u_{in} = 0.3$ mm/s. This is because the strength of the imposed upflow is larger than that of the downflow in the vicinity of the cold wall. Thus, the secondary convective cell is swept by the imposed upflow. As indicated in Figs. 2d, 3d, and 3d, vapor flows primarily upward and away from the heated wall where the vapor is generated, and is condensed by the incoming subcooled liquid.

The variations of the liquid saturation along the heated wall for the porous medium of $d_p = 0.8$ mm at $q_w = 15$ kW/m^2 for different values of inlet velocities are displayed in Fig. 5. Generally, for any values of the inlet velocity, the liquid phase ($s_w = 1$) exists in the entrance length and the liquid saturation drops gradually along the heated surface, reaching a minimum value at the exit of the channel. This implies that the dryout point, if it occurs, will always be on the wall at the exit of the channel for the aiding flow. It is also evident from Fig. 5 that the liquid saturation along the heated surface decreases as the strength of the aiding flow is weakened.

The effect of the particle diameter on the liquid-saturation distribution along the heated surface for $u_{in} = 0.15$ mm/s and at $q_w = 15$ kW/m^2 is illustrated in Fig. 6. It is seen that the larger particle sizes give a higher liquid saturation, implying that under the same condition dryout occurs earlier in a packed channel with smaller particles. This is because the motion of the liquid phase is affected by the particle diameters. A small particle diameter leads to a larger drag force in the two-phase region due to higher vapor viscosity, even though the capillary pressure can be increased slightly. For this reason, the mass flux of the subcooled liquid is decreased with

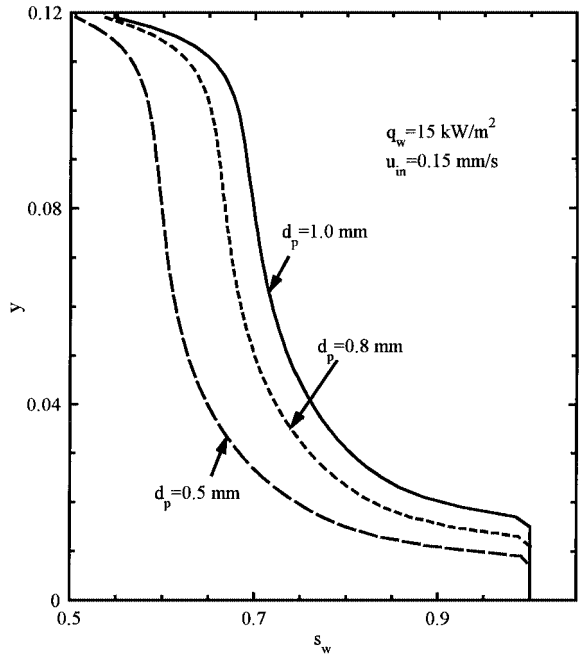

Fig. 6 Effect of the particle diameters on the minimum liquid saturation for the aiding flow.

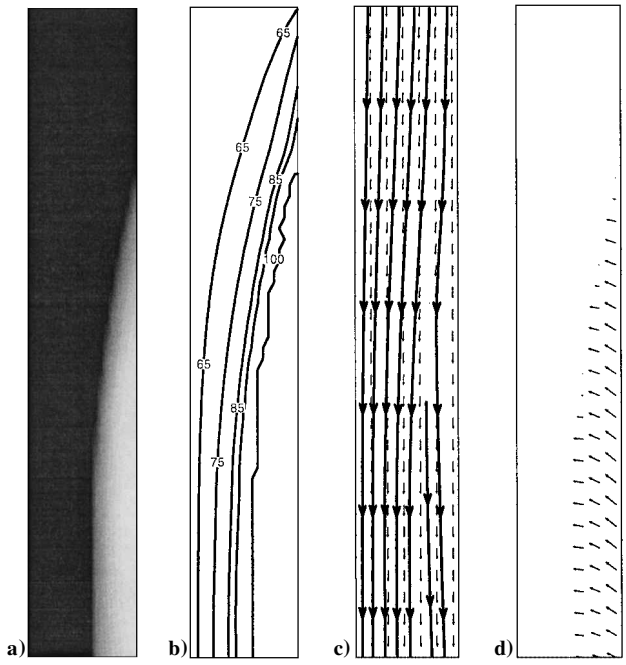

Fig. 7 Distributions of a) liquid saturation, b) isotherms (in °C), c) vapor velocity, and d) liquid velocity for the opposing flow: u_{in} = −0.3 mm/s at q_w = 15 kW/m^2 and d_p = 0.8 mm.

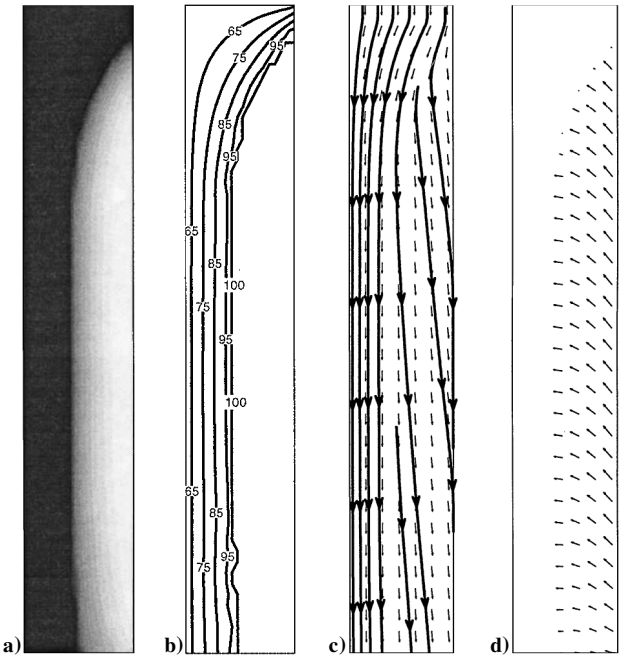

Fig. 8 Distributions of a) liquid saturation, b) isotherms (in °C), c) vapor velocity, and d) liquid velocity for the opposing flow: u_{in} = −0.1 mm/s at q_w = 15 kW/m^2 and d_p = 0.8 mm.

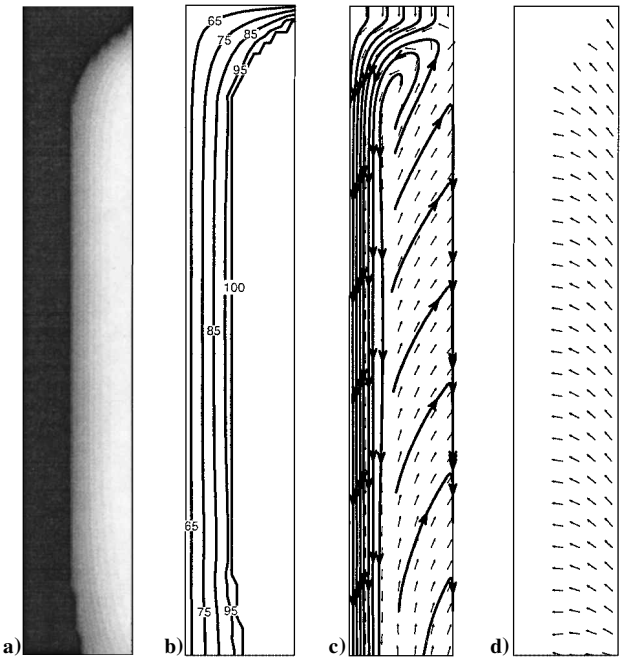

Fig. 9 Distributions of a) liquid saturation, b) isotherms (in °C), c) vapor velocity, and d) liquid velocity for the opposing flow: u_{in} = −0.05 mm/s at q_w = 15 kW/m^2 and d_p = 0.8 mm.

the increase of the particle diameter. Thus, the channel packed with particles of a larger diameter gives a higher dryout heat flux.

Opposing Flow

Figures 7–9 illustrate the distributions of the liquid saturation, the isotherms, as well as the velocities for both liquid and vapor in the capillary structure for $d_p = 0.8$ mm at $q_w = 15$ kW/m^2 as the inlet velocity of the opposing flow is increased from $u_{in} = -0.4$ mm/s, -0.2 mm/s, and -0.08 mm/s. For the opposing flow, both the distribution of liquid saturation and isotherms show that a two-phase zone exists in the right-lower portion of the capillary structure, whereas the working fluid is in the liquid phase in the left-upper portion of the structure. From the liquid-saturation distributions and the isotherms shown in Figs. 7a, 8a, and 9a, as well as Figs. 7b, 8b, and 9b, it is also noted that as the strength of the opposing flow becomes strong, the two-phase zone contracts while the subcooled liquid zone expands downward due to the cooling effect from the incoming subcooled liquid from the top. The liquid velocity fields show that the liquid flows primarily downward when the strength of the opposing flow is strong (Figs. 7c and 8c). However, it is interesting to note that when the opposing flow becomes weak (Fig. 9c), the liquid adjacent to the cold wall continues moving downward, whereas the liquid phase in the two-phase zone near the heated surface moves upward. This buoyancy-induced liquid-phase upflow is counteracted by the opposing flow at the inlet (the top of the capillary structure). As a result,

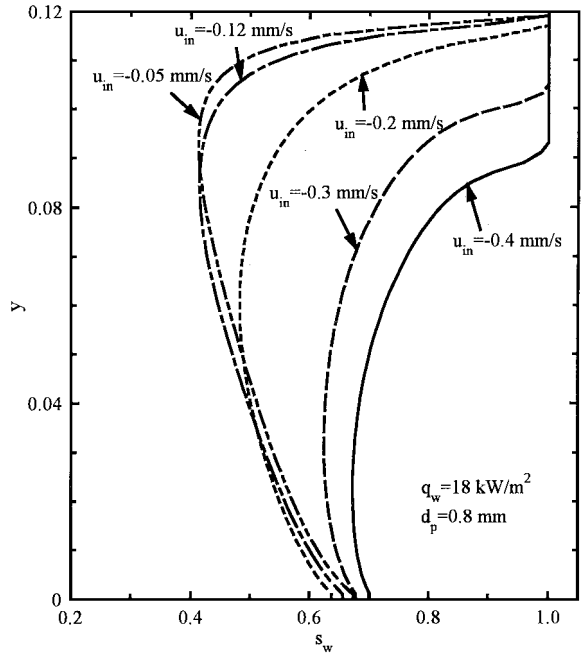

Fig. 10 Liquid saturation distribution along the heated wall for various opposing flow velocities: $u_{in} = -0.05$, -0.12, -0.2, -0.3, and -0.4 mm/s at $q_w = 18$ kW/m^2 and $d_p = 0.8$ mm.

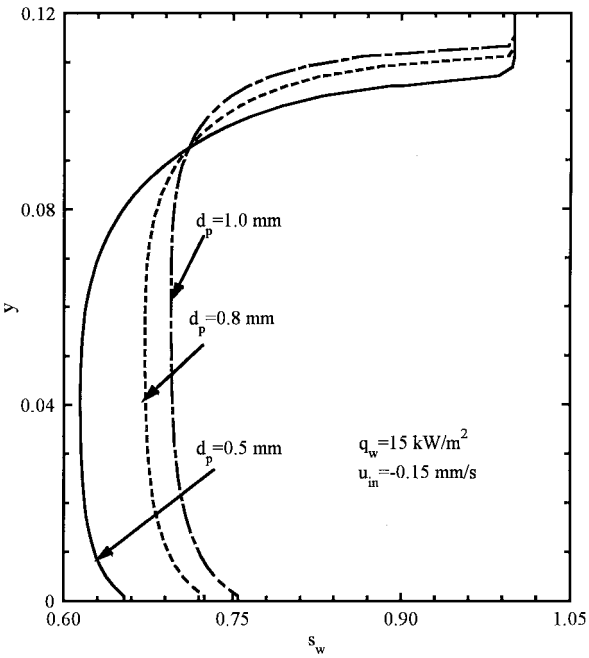

Fig. 11 Effect of the particle diameters on the minimum liquid saturation for the opposing flow.

a closed recirculation loop is formed near the top of the capillary structure (Fig. 9c).

The variations of the liquid saturation along the heated wall for the porous medium of $d_p = 0.8$ mm at $q_w = 15$ kW/m^2 for various inlet velocities of the opposing flow are displayed in Fig. 10. In comparison with the situation for the aiding flow shown in Fig. 5, the variation of the liquid saturation for the opposing flow is somewhat different. It is seen that the liquid saturation is kept at $s_w = 1$ in the entrance region (the top side), and, it begins to drop while flowing down along the heated surface, reaches a minimum, and increases slightly at the exit of the channel (the bottom side). It is noted that when the strength of the opposing flow is strong ($u_{in} = -0.3$ and -0.4 mm/s), the minimum liquid saturation locates somewhere near the exit of the capillary structure. As the opposing flow velocity is decreased, the buoyancy-inducedupflow becomes more significant. As a result, the value of the minimum saturation in the heated surface drops. The location of the minimum liquid saturation moves up and occupies a wider area in the heated surface. The effect of the particle diameter on the liquid-saturation distribution along the heated surface for $u_{in} = -0.15$ mm/s and at $q_w = 15$ kW/m^2 is illustrated in Fig. 11. Similar to the situation for the aiding flow, it is seen that for the opposing flow, the larger particle sizes also give a higher liquid saturation.

Conclusion

Numerical solutions are obtained for mixed convective boiling heat transfer subjected to either aiding or opposing flows in a vertically oriented capillary porous structure with asymmetric heating of opposing walls. Liquid-saturation distributions, isotherms, as well as liquid and vapor velocity fields, are presented. The liquid velocity distributions for both aiding and opposing flows indicate the existence of a secondary convective cell adjacent to the cold wall when the strength of the imposed flow is small. It is found that for the case of the aiding flow, the minimum liquid saturation always occurs at the exit of the packed channel. For the case of the opposing flow, however, the minimum liquid saturation usually locates somewhere close to the exit of the heated wall and it moves upward along the wall as the strength of the imposed opposing flow is weakened. Numerical results also indicate that larger particles give higher dryout heat flux for both the aiding and the opposing flow.

Acknowledgments

This work was supported by Hong Kong Research Grant Council Earmarked Research Grants HKUST 809/96E and HKUST 814/96E.

References

[1] Wooding, R. A., "Convection in Saturated Porous Medium at Large Rayleigh Number and Peclet Number," *Journal of Fluid Mechanics*, Vol. 15, Pt. 4, 1963, pp. 527–544.

[2] Sutton, M., "Onset of Convection in a Porous Channel with Net Through Flow," *Physics of Fluids*, Vol. 13, No. 8, 1970, pp. 1931–1934.

[3] Lai, F. C., Prasad, V., and Kulacki, F. A., "Aiding and Opposing Mixed Convection in a Vertical Porous Layer with a Finite Wall Heat Source," *International Journal of Heat and Mass Transfer*, Vol. 31, No. 5, 1988, pp. 1049–1061.

[4] Choi, C. Y., Lai, F. C., and Kulacki, F. A., "Mixed Convection in Vertical Porous Annuli," *Heat Transfer Philadelphia, American Institute of Chemical Engineers Symposium Series*, Vol. 85, No. 269, 1989, pp. 356–361.

[5] Pu, W. L., Cheng, P., and Zhao, T. S., "An Experimental Study of Mixed Convection Heat Transfer in a Vertical Packed Channel Heated Asymmetrically," *Journal of Thermophysics and Heat Transfer* (to be published).

[6] Wang, C. Y., Beckermann, C., and Fan, C., "Numerical Study of Boiling and Natural Convection in Capillary Porous Media Using the Two-Phase Mixture Model," *Numerical Heat Transfer A*, Vol. 26, No. 4, 1994, pp. 375–398.

[7] Wang, C. Y., and Cheng, P., "Multiphase Flow and Heat Transfer in Porous Media," *Advances in Heat Transfer*, Vol. 30, 1997, pp. 93–196.

[8] Easterday, O. T., Wang, C. Y., and Cheng, P., "A Numerical and Experimental Study of Two-Phase Flow and Heat Transfer in a Porous Formation with Localized Heating from Below," *Proceedings of American Society of Mechanical Engineers, Heat Transfer and Fluid Engineering Divisions*, HTD Vol. 321, American Society of Mechanical Engineers, New York, 1995, pp. 723–732.

[9] Peterson, G. P., and Chang, C. S., "Two-Phase Heat Dissipation Utilizing Porous-Channels of High-Conductivity Material," *Journal of Heat Transfer*, Vol. 120, No. 1, 1998, pp. 243–252.

[10] Wang, C. Y., "Modeling of Capillary Evaporators," *Proceedings of the International Conference on Porous Media and Their Applications in Science, Engineering and Industry*, Kona, HI, 1996, pp. 602–627.

[11] Udell, K. S., "Heat Transfer in Porous Media Considering Phase Change and Capillary—The Heat Pipe Effect," *International Journal of Heat and Mass Transfer*, Vol. 28, No. 2, 1985, pp. 485–495.

[12] Patankar, S. V., *Numerical Heat Transfer and Fluid Flow*, Taylor and Francis, Washington, DC, 1980.

[13] Nield, D. A., and Bejan, A., *Convection in Porous Media*, Springer–Verlag, New York, 1992.

[14] Zehner, P., and Schlünder, E. U., "Thermal Conductivity of Granular Materials at Moderate Temperatures," *Chemie Ingenieur Technik*, Vol. 42, No. 14, 1970, pp. 933–941.